



 Cite this: *RSC Adv.*, 2020, 10, 34231

# Elucidating the effect of precursor decomposition time on the structural and optical properties of copper(II) nitride nanocubes†

 Rudo Kadzutu-Sithole,<sup>a</sup> Lerato F. E. Machogo-Phao,<sup>a</sup> Tshwarela Kolokoto,<sup>a</sup> Memory Zimuwandeyi,<sup>a</sup> Siziwe S. Gqoba,<sup>a</sup> Kalenga P. Mubiayi,<sup>a</sup> Makwena J. Moloto,<sup>b</sup> Juanita Van Wyk<sup>\*a</sup> and Nosipho Moloto<sup>b</sup>  <sup>\*a</sup>

To study the effect of time on the colloidal synthesis of Cu<sub>3</sub>N nanoparticles, copper(II) nitrate was thermally decomposed at 260 °C for up to 60 min in octadecylamine as a stabilizing ligand. Thermolysis of the nitrate followed four steps which included; nucleation, growth, ripening and decomposition. At 5 min, partially developed nanocubes were found in a dense population of Cu<sub>3</sub>N nuclei. Well-defined Cu<sub>3</sub>N nanocubes were obtained at 15 min with no presence of the nuclei. TEM images showed disintegration of the cubes at 20 min and as time progressed, all the Cu<sub>3</sub>N decomposed to Cu by 60 min. The formation of the Cu<sub>3</sub>N nanocubes was confirmed by XRD and XPS. FTIR suggested the formation of a nitrile (RCN) as a result of the thermal decomposition in octadecylamine (ODA) and this was confirmed using NMR and hence, a reaction mechanism was then proposed. The optical properties of the as-synthesized Cu<sub>3</sub>N were studied using UV-vis and photoluminescence spectroscopies. The absorption spectra for particles synthesized from 5 min to 15 min showed a singular exciton peak while from 20 min to 60 min two peaks were observed. The two peaks may both be associated with the two direct transitions observed in Cu<sub>3</sub>N or the more red-shifted peak could be a result of localized surface plasmon resonance due to the Cu nanoparticles. Nevertheless, similar to other studies, it is clear that the optical properties of Cu<sub>3</sub>N are complex.

Received 15th November 2019

Accepted 16th August 2020

DOI: 10.1039/c9ra09546b

[rsc.li/rsc-advances](http://rsc.li/rsc-advances)

## 1. Introduction

The industrial application of semiconducting nanomaterials cannot be overemphasized, more especially in photonics and medicine. Colloidal synthesis of Cu<sub>3</sub>N continues to receive tremendous research focus marking a variation from the popular solid-state methods which involve the use of RF magnetron sputtering. In literature, there are many discrepancies in the data that have been reported for Cu<sub>3</sub>N nanoparticles (NPs). For example, the band gap and thermal stability and this has been attributed to the unstable nature of Cu<sub>3</sub>N acquired during the growth stage.<sup>1</sup> Researchers are slowly turning their focus to solution-based synthesis of Cu<sub>3</sub>N NPs due to the ease with which the desired morphology and properties of the NPs can be engineered. Few reports have demonstrated that Cu<sub>3</sub>N NPs can be synthesized by employing ammonolysis

or use of N sources such as azide, hexamethylenetetramine and urea but the challenge with these methods is that the resultant NPs are ill-shaped.<sup>2–8</sup> Special attention is recently being given to the synthesis of Cu<sub>3</sub>N NPs using direct thermal decomposition of Cu(NO<sub>3</sub>)<sub>2</sub>·3H<sub>2</sub>O in octadecylamine (ODA) to obtain well defined nanocubes.<sup>9–13</sup> Thermal decomposition of other metal nitrates for example, Mn(NO<sub>3</sub>)<sub>2</sub>, Ni(NO<sub>3</sub>)<sub>2</sub>·6H<sub>2</sub>O, Zn(NO<sub>3</sub>)<sub>2</sub>·6H<sub>2</sub>O, Ce(NO<sub>3</sub>)<sub>3</sub>·6H<sub>2</sub>O, Co(NO<sub>3</sub>)<sub>2</sub>·6H<sub>2</sub>O in ODA resulted in the formation of corresponding metal oxides and not metal nitrides.<sup>14</sup> Wang *et al.*<sup>11</sup> demonstrated that it is very crucial to control the concentration of Cu(NO<sub>3</sub>)<sub>2</sub> in ODA in order to get Cu<sub>3</sub>N and not Cu or its oxides. Xi *et al.*<sup>13</sup> reported on the formation of Cu<sub>3</sub>N upon decomposing Cu(NO<sub>3</sub>)<sub>2</sub> in a mixture of two reducing agents, ODA and oleylamine (OLA) at 240 °C for up to 10 min. The report revealed that very few cubes were observed amongst small nuclei of Cu<sub>3</sub>N after 2 min but only cubes were present after 10 min. However, the authors did not report on the effect of time beyond 10 min. Herein, we probe the effect of precursor decomposition time on the formation of Cu<sub>3</sub>N nanocubes through thermolysis of Cu(NO<sub>3</sub>)<sub>2</sub> at 260 °C for up to 60 min in ODA as the capping and reducing agent. Progression in the formation of the Cu<sub>3</sub>N nanocubes could be summarized in four stages namely; nucleation, growth, ripening and decomposition. In order to verify our findings, the same

<sup>a</sup>Molecular Sciences Institute, School of Chemistry, University of the Witwatersrand, Private Bag 3, Wits, 2050, South Africa. E-mail: Juanita.VanWyk@wits.ac.za; Nosipho.Moloto@wits.ac.za; Fax: +27117176749; Tel: +27117176732; +27117176774

<sup>b</sup>Department of Chemistry, Faculty of Applied and Computer Science, Vaal University of Technology, Private Bag X021, Vanderbijlpark, South Africa

† Electronic supplementary information (ESI) available. See DOI: 10.1039/c9ra09546b



synthetic procedure was followed using hexadecylamine (HDA) as the capping and reducing agent.

## 2. Experimental section

### Materials

Copper(II) nitrate trihydrate (puriss. p. a, 99–104%), 97% octadecylamine (ODA), octadecene ( $\geq 95.0\%$  GC), 98% hexadecylamine (HDA), 99.5% chloroform and ethanol absolute ( $\geq 99.8\%$  GC) were purchased from Sigma-Aldrich. Chloroform was refluxed in calcium hydride and distilled in nitrogen before use and ethanol was stored under 3A molecular sieves. All other chemicals were used as received.

### Synthesis of $\text{Cu}_3\text{N}$ nanoparticles

The controlled synthesis of  $\text{Cu}_3\text{N}$  nanoparticles was achieved by thermal decomposition of copper(II) nitrate in ODA.  $\text{Cu}(\text{NO}_3)_2 \cdot 3\text{H}_2\text{O}$  (1 mmol) was dissolved in octadecene (1 mL), mixed with ODA (10 mL) and degassed under a continuous flow of  $\text{N}_2$  gas (©Afrox, 99.997%) at  $110^\circ\text{C}$ . After an hour, the temperature was slowly raised to  $260^\circ\text{C}$ . Aliquots were then extracted at 5, 10, 15, 20, 30 and 60 min. Dry absolute ethanol was then added to the aliquots to flocculate the particles. The particles were then collected by centrifugation at 5000 rpm. The samples were then dissolved in dry chloroform, flocculated using dry absolute ethanol and centrifuged 5 times. The final powder samples were dried in a vacuum oven and kept under inert conditions before characterization.

### Characterization

A Varian Cary Eclipse (Cary 50) UV-vis spectrophotometer was used to carry out the optical properties of the NPs. The photoluminescence spectra of the NPs were recorded on a Varian Cary Eclipse EL04103870 spectrofluorometer with a medium PMT voltage at an excitation wavelength of 200 nm. The absorption and emission spectra were obtained in chloroform and placed in quartz cuvettes (1 cm path length). Powdered XRD patterns of the samples were measured on a Bruker MeasSrv D2-205530 diffractometer using secondary graphite monochromated  $\text{Cu K}\alpha$  radiation ( $\lambda$  1.5406 Å) at 30 kV/30 mA. Measurements were taken using a glancing angle of incidence detector at an angle of  $2^\circ$ , for  $2\theta$  values over  $10$ – $90^\circ$  in steps of  $0.026^\circ$  with a step time of 37 s and at a temperature of  $25^\circ\text{C}$ . X-ray photoelectron spectroscopy measurements were performed with a PHI 5000 Versaprobe – Scanning ESCA Microprobe operating with a  $100\ \mu\text{m}$  25 W 15 kV Al monochromatic X-ray beam. The transmission electron microscopy (TEM) was carried out on a FEI Technai T12 operated at an acceleration voltage of 200 kV with a beam spot size of 20–100 nm in TEM mode. The vibrational modes were measured on a Bruker Tensor 27 FT-IR and the nuclear magnetic resonance (NMR) data was obtained using a 500 MHz Bruker AVANCE III, the samples were run using  $\text{CDCl}_3$  as a solvent at 300 K.

## 3. Results and discussion

Powder X-ray diffraction was used to determine the crystal phases of the resultant NPs and for the detection of any

impurities. Shown in Fig. 1 are the XRD patterns of the NPs synthesized from 5 min to 60 min in ODA as well as the reference patterns of  $\text{Cu}_3\text{N}$  and possible impurities. The series of Bragg reflections in the experimental patterns show peaks that correspond to planes (100), (110), (111), (200), (210), (211) and (220) of the cubic phase of  $\text{Cu}_3\text{N}$  (card number JCPDS card no.: 86-2283). An additional peak from the 20 min sample is observed at  $2\theta = 42.98^\circ$  showing the initial stage of Cu formation. More copper peaks emerge till all the  $\text{Cu}_3\text{N}$  is converted to Cu (JCPDS card no.: 04-0836) at 60 min. These sets of data show that thermal decomposition of  $\text{Cu}(\text{NO}_3)_2$  in ODA at  $260^\circ\text{C}$  result in the formation of  $\text{Cu}_3\text{N}$  after about 5 min.  $\text{Cu}_3\text{N}$  continues to be the only product present until about 20 min, then a mixture of  $\text{Cu}_3\text{N}$  and Cu NPs begin to form until only Cu is detected at 60 min. Understanding of the metallization of  $\text{Cu}_3\text{N}$  can come in handy in making microscopic Cu metallic links during the fabrication of optical recording media<sup>15</sup> and optical data storage.<sup>16</sup> The peak assigned as # is associated with the degradation products of ODA and the corresponding XRD patterns are shown in Fig. 1S.† In addition, no oxide impurities were observed from the XRD.

The composition of the formed  $\text{Cu}_3\text{N}$  NPs and oxidation states of Cu and N was further confirmed by employing X-ray photoelectron spectroscopy (XPS) and the results are shown in Fig. 2 and 3. From the survey spectrum, it can be deduced that the as-synthesized  $\text{Cu}_3\text{N}$  NPs contain C, O, N and Cu. Majumdar *et al.*<sup>17</sup> discovered that  $\text{Cu}_3\text{N}$  films that were synthesized by RF magnetron sputtering consisted of 20.4% C and 35.5% O after being exposed to air. As such, exposure of the as-synthesized  $\text{Cu}_3\text{N}$  NPs to air and the presence of the organic stabilizer could explain the observed pivotal amount of C and O in the sample as seen in Fig. 2. The copper auger peak (Cu LMM) is indicative of the presence of  $\text{Cu}^{2+}$ , this suggests the presence of CuO which is a readily observed impurity in  $\text{Cu}_3\text{N}$  due to the oxidation. The XRD in Fig. 1 however showed no evidence of CuO, suggesting only surface oxidation. Two peaks centralized at 285.35 and 285.95 eV from the C 1s high-resolution are assigned to C–C and C–O respectively. The C–C is due to the long chain alkylamine capping agent. The presence of C–O is attributed to the oxidation of the capping agent as later shown in the FTIR results (Fig. 6). The O 1s spectrum has a broad peak that is centered at 532.04 eV and deconvolution of the O 1s spectrum gives rise to two peaks at 531.87 and 533.36 eV that are ascribed to the presence of C–O and metal–O specie respectively.<sup>12</sup> The C–O further confirms the oxidation of the capping agent while the metal–oxygen bonded specie is indicative of the formation of CuO.

The NPs were synthesized in a nitrogen-rich atmosphere and the N 1s high-resolution XPS depicts the main peak centered at 399.70 eV showing the main bonding of nitrogen to copper (N–Cu) in the  $\text{Cu}_3\text{N}$  nanocubes. This value is higher than the 397.7 eV that has been reported.<sup>18–22</sup> The peak at 403.01 eV is attributed to N–C bonding in stearonitrile. Interestingly, Navio *et al.* and others were of the idea that the 397.7 eV peak is attributed to the presence of nitrogen that is adsorbed to the surface of the  $\text{Cu}_3\text{N}(100)$  and the second peak that they

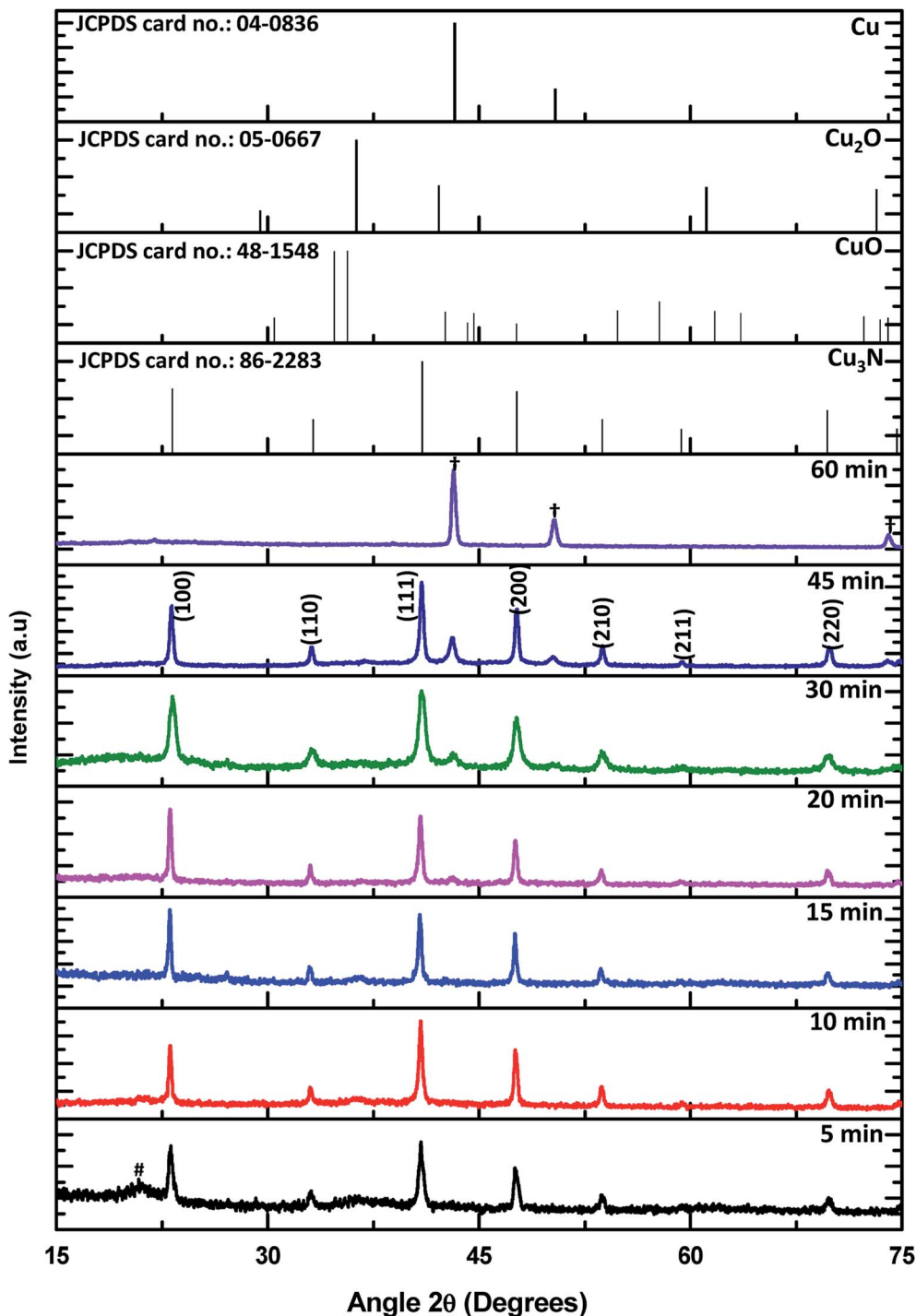


Fig. 1 Powder XRD diffractograms of  $\text{Cu}_3\text{N}$  NPs obtained after 5, 10, 15, 20, 30, 45 and 60 min at 260 °C in ODA as well as the standard patterns of  $\text{Cu}_3\text{N}$ ,  $\text{CuO}$ ,  $\text{Cu}_2\text{O}$  and  $\text{Cu}$ . The symbol (†) shows peaks for  $\text{Cu}$  and (#) decomposition product of the capping agent.

obtained at 398.7 eV was attributed to the presence of N that is in the bulk of the  $\text{Cu}_3\text{N}$ .<sup>20,23</sup>

In the Cu 2p spectrum, the expected  $\text{Cu}^+$  peaks were obtained at 933.48 eV and 953.52 eV of the Cu  $2p_{3/2}$  and Cu  $2p_{1/2}$  states respectively, consistent with previous reports.<sup>24</sup> Corresponding shakeup peaks at around 934.4 and 954.63 eV (ref. 24) were not obtained hence suggesting the lack of  $\text{Cu}^{2+}$  in the NPs. However,

a peak of relatively lower intensity was obtained around 963.20 eV and reports<sup>25–27</sup> have associated this peak as a shakeup peak to Cu  $2p_{1/2}$  suggesting the presence of  $\text{CuO}$ . In the XRD pattern, there were no evident peaks that could be ascribed to  $\text{CuO}$  hence, the detected oxide in the  $\text{Cu}_3\text{N}$  nanocubes could be a result of mild surface oxidation due to exposure to atmospheric oxygen.

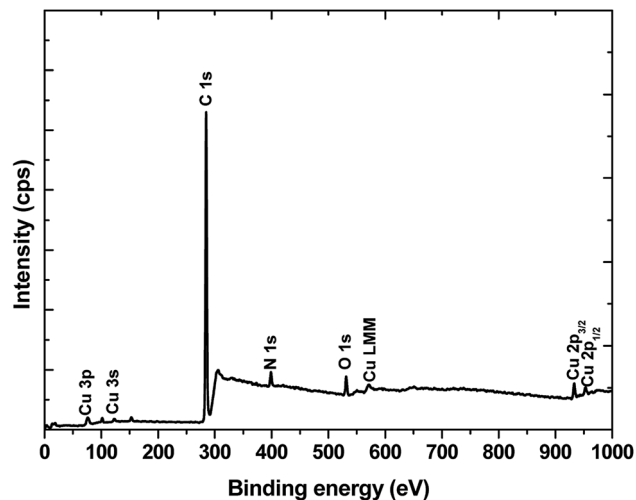


Fig. 2 XPS wide scan of  $\text{Cu}_3\text{N}$  NPs (15 min sample).

To study the morphology of the as-synthesized NPs, the powders were dispersed in chloroform and drop-casted onto Cu and Ni grids. After drying, they were then analyzed and imaged under the transmission electron microscope and the images are

shown in Fig. 4. The images obtained show that the sample that is collected after 5 min at  $260^\circ\text{C}$  consists of mixed morphology. Relatively few nanocubes are found in between a cloud of very small dot-like NPs. A closer look reveals that some of the nanocubes are incompletely formed and in close contact with a number of the dot-like NPs. In another study, Xi *et al.* obtained a similar mixture of nuclei and cubes after 5 min of thermal decomposition of  $\text{Cu}(\text{NO}_3)_2$  in a mixture of ODA and oleylamine at  $240^\circ\text{C}$ .<sup>13</sup>

At 10 min, there is a much greater population of the nanocubes and much less of the dot-like NPs and the nanocubes are much more defined and show some degree of self-assembly. The 'dots' can still be seen and some are found on and in between the cubes and on the edges of the cubes hence making it slightly difficult to measure the size of the cubes as some of them do not possess well-defined edges, nevertheless, the average size is estimated to be  $41 \pm 6.2$  nm. The 15 min sample brings about a change in composition. The nanocubes are aligned next to each other resembling a pattern of layered bricks. The dot-like NPs are almost non-existent and the edges of the cubes are well-defined with no evidence of dots on them. These are then named 'perfect nanocubes' and measurement of their edges gives a size of  $39 \pm 8.4$  nm. At 20 min of synthesis,

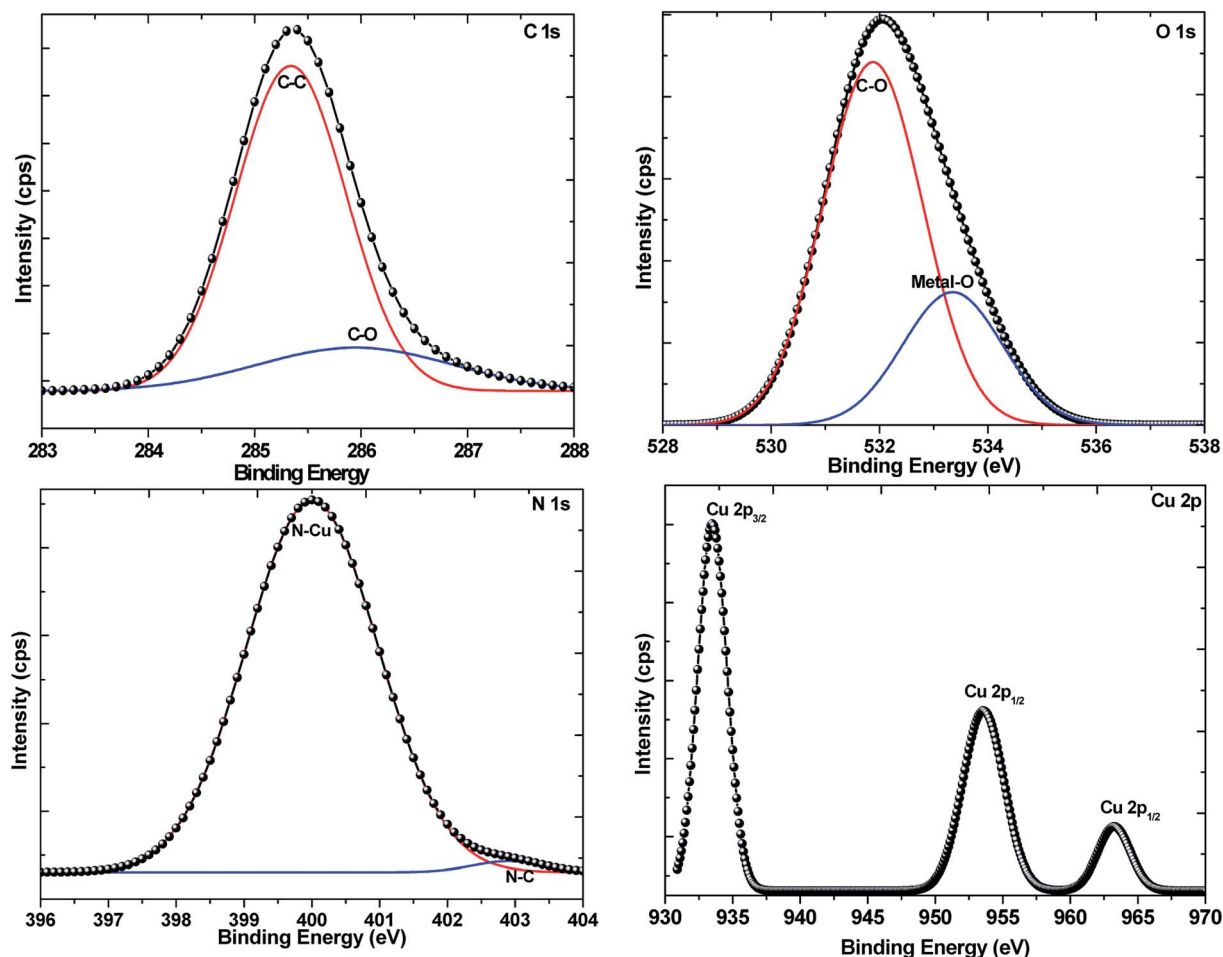


Fig. 3 High-resolution spectra of  $\text{Cu}_3\text{N}$  NPs with focus on C 1s, O 1s, N 1s, and Cu 2p.

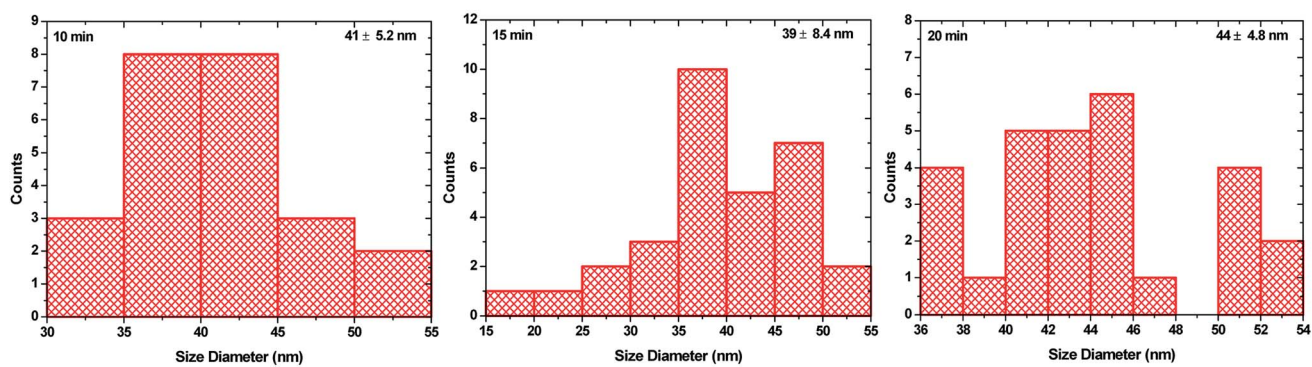
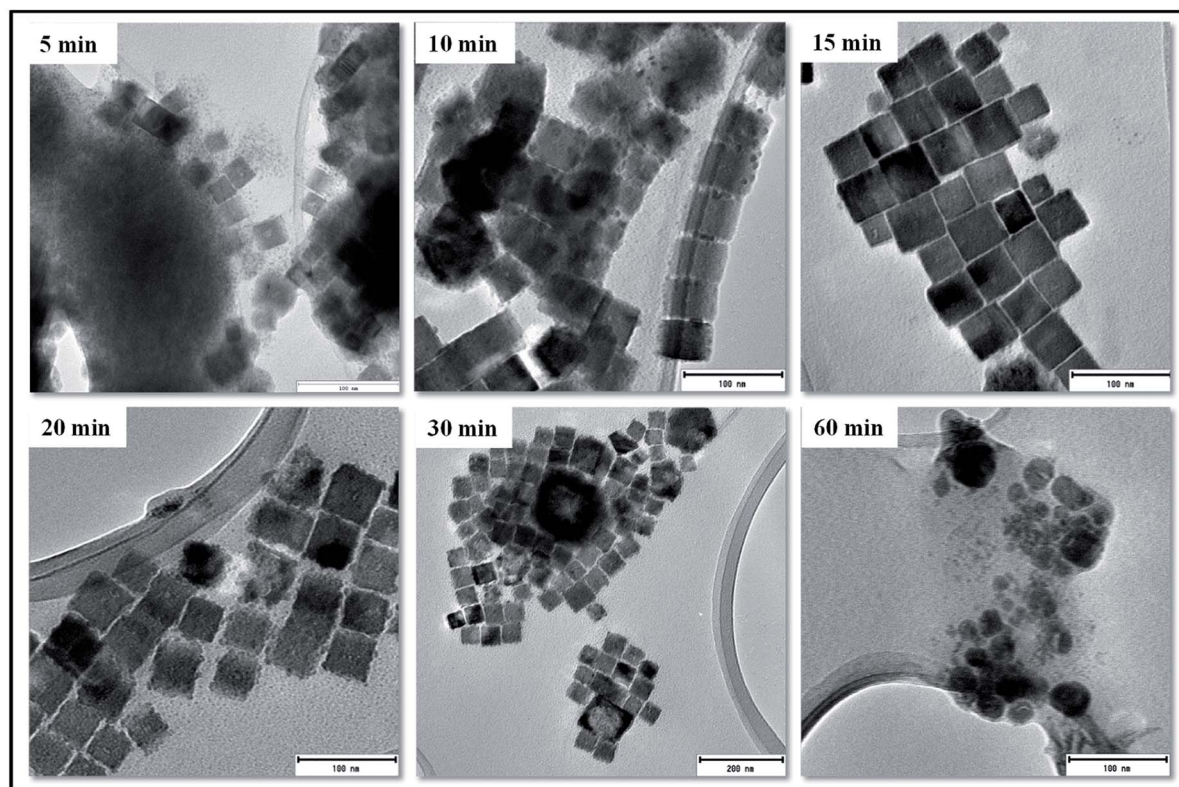


Fig. 4 TEM images of  $\text{Cu}_3\text{N}$  NPs obtained after 5, 10, 15, 20, 30 and 60 min in ODA and size distribution for 10, 15 and 20 min samples.

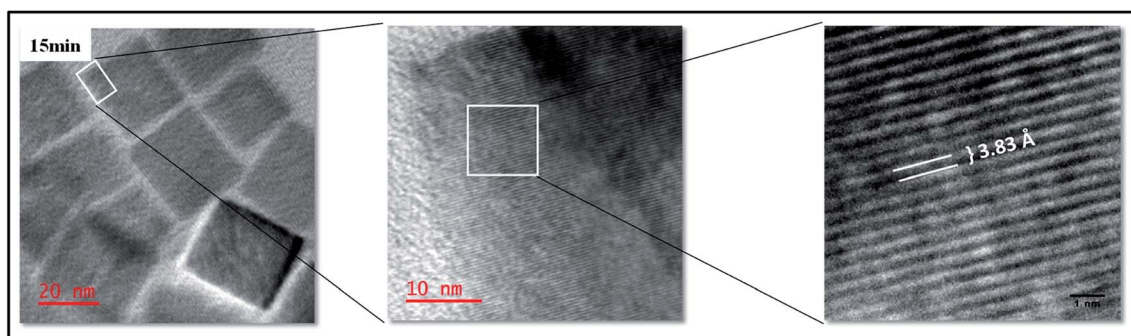


Fig. 5 HRTEM of  $\text{Cu}_3\text{N}$  NPs synthesized after 15 min in ODA.

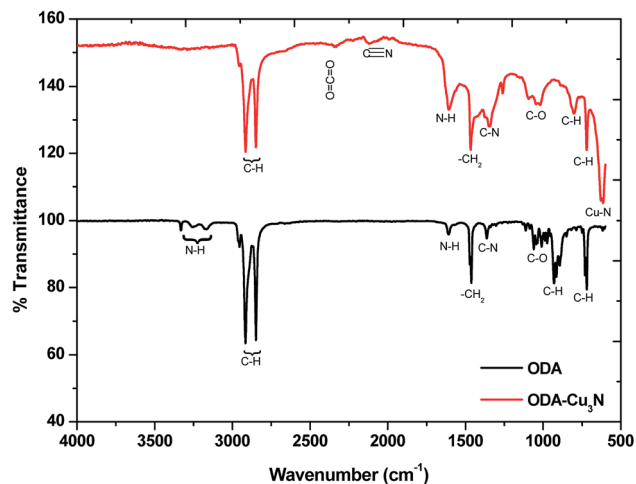


Fig. 6 FTIR spectra of the 15 min synthesized raw ODA and  $\text{Cu}_3\text{N}$  NPs.

the ‘perfect nanocubes’ are no longer perfect however, the sizes can still be estimated at  $44 \pm 4.8$  nm. They look like they are crumbling and the edges start having the dot-like NPs again. At this stage, XRD shows the emergence of a peak around  $2\theta = 50.6^\circ$  that is assigned to Cu. Attempted measurements of the

edges gives a rough estimate of 44 nm and no further measurements are taken thereafter as the nanocubes have no well-defined shapes. The break down of the nanocubes continues and by 30 min, the breakdown cubes seem to affect the neighbouring cubes resulting in the formation of giant cube-like structures with hollow interiors. At this stage, Cu related peaks can be seen on the XRD pattern although they are of very low intensity compared to the  $\text{Cu}_3\text{N}$  peaks. By 60 min, no cubes can be seen but polydispersed nanoparticles are obtained and the XRD shows peaks that are all ascribed to Cu and there is no evidence of peaks that can be associated with  $\text{Cu}_3\text{N}$ .

Shown in Fig. 5 are the HRTEM images of the perfect nanocubes. The nanocubes have lattice fringes with the  $d$ -spacing of 3.83 Å corresponding to the (100) plane of the anti- $\text{ReO}_3$  cubic structure of  $\text{Cu}_3\text{N}$ . This is consistent with the results obtained in the X-ray diffraction in Fig. 1.

To investigate the coordination of the ligand, Fourier transform infra-red (FTIR) spectroscopic analysis was performed. The spectrum that is obtained from the nanoparticles synthesized in 15 min is compared with that of raw ODA (Fig. 6). Generally, the results show that the  $\text{Cu}_3\text{N}$  NPs are capped by the organic ligand, as the corresponding vibrations in ODA are detected on the synthesized NPs. The characteristic C-H stretching vibrations are obtained from  $2845 \text{ cm}^{-1}$  to  $2959 \text{ cm}^{-1}$

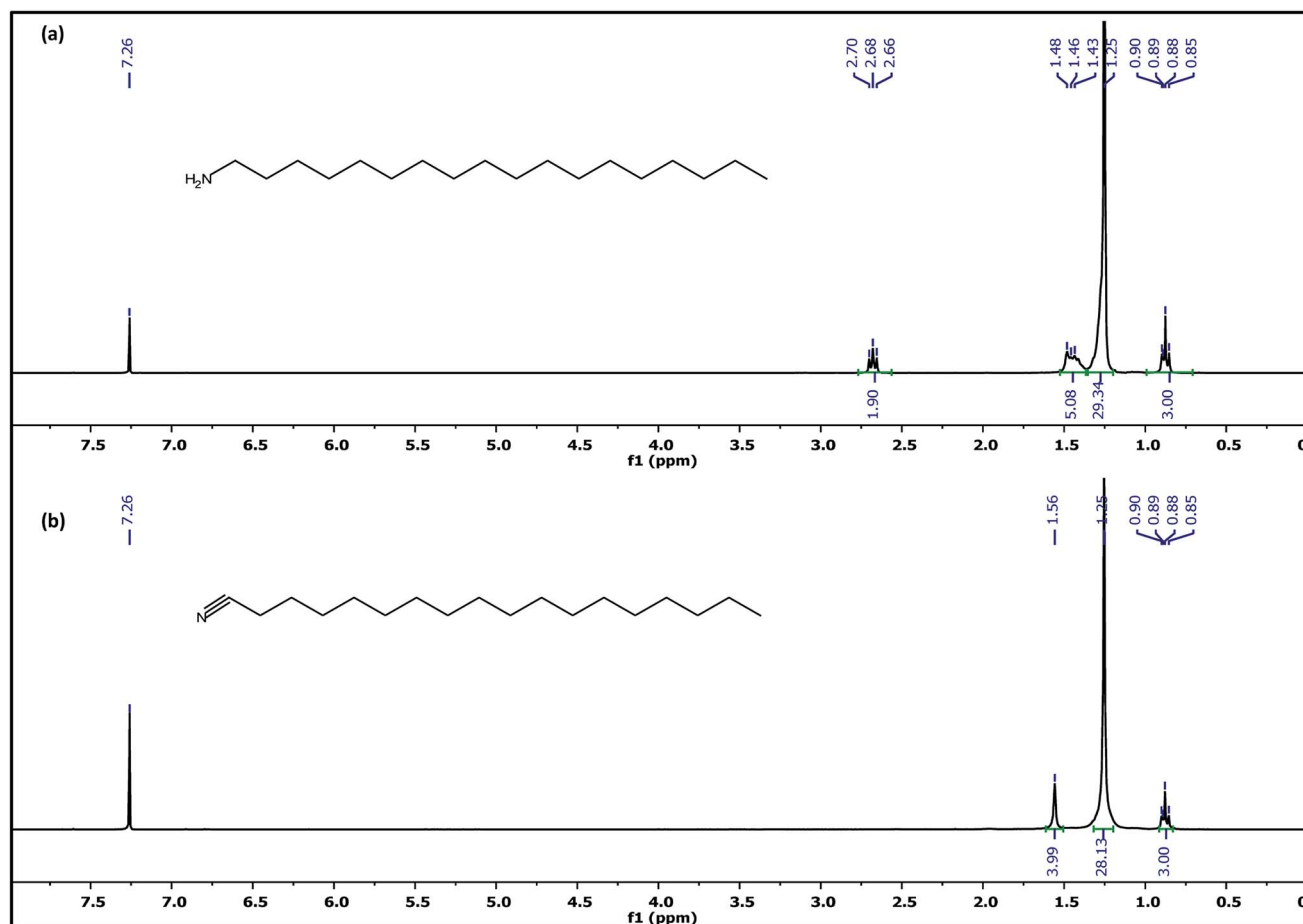


Fig. 7  $^1\text{H}$  NMR spectra of (a) ODA and (b)  $\text{Cu}_3\text{N}$  nanocubes in  $\text{CDCl}_3$  (15 min sample).

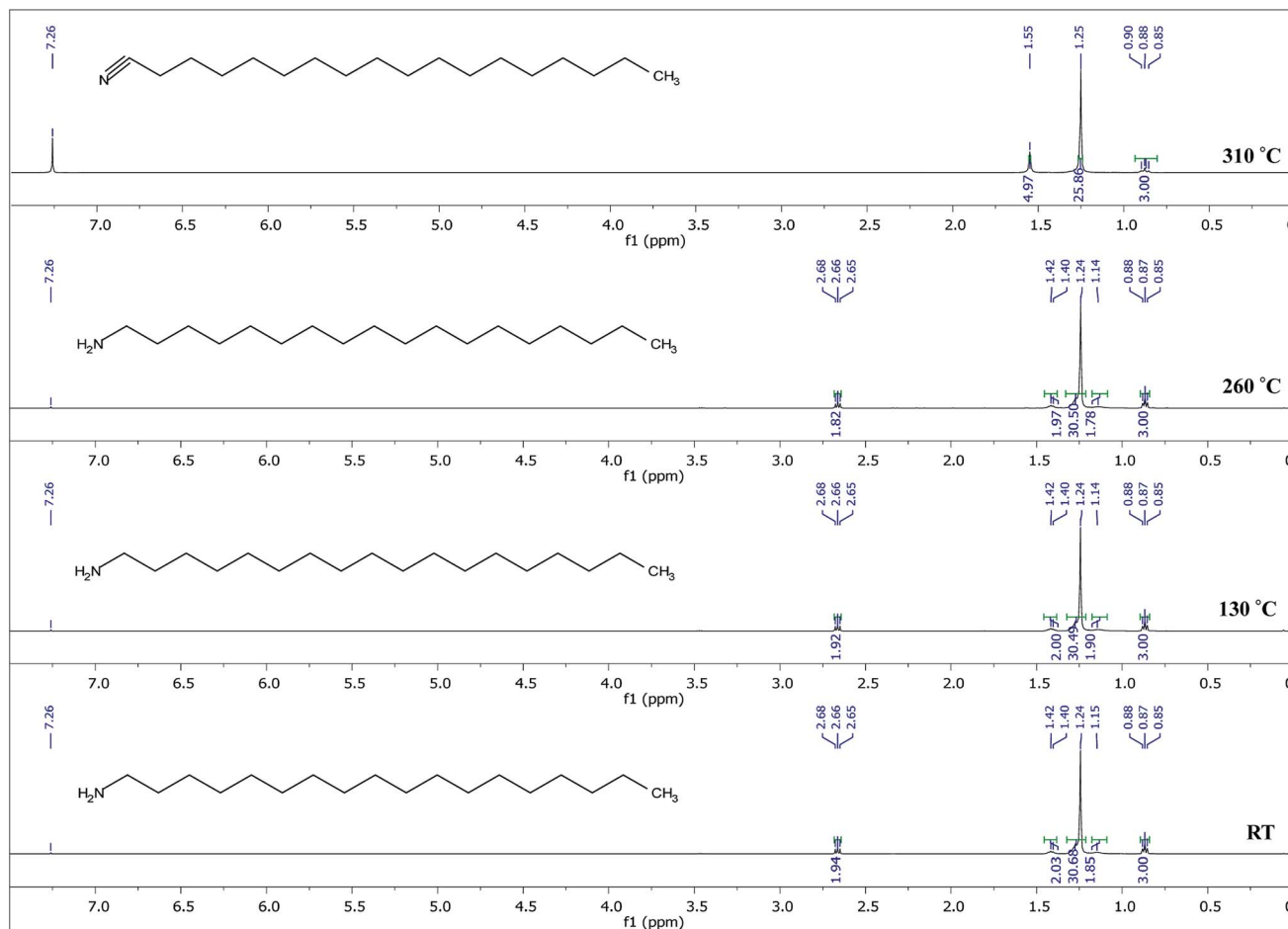


Fig. 8  $^1\text{H}$  NMR spectra of ODA heated from RT to 260  $^\circ\text{C}$  for 15 min and heated at 310  $^\circ\text{C}$  for 32 h.

and the  $-\text{CH}_2$  bending vibration at  $1460\text{ cm}^{-1}$  is slightly shifted from the  $1465\text{ cm}^{-1}$  in ODA showing that the chemical environment has slightly changed due to the coordination. The peak at  $2335\text{ cm}^{-1}$  for the ODA capped  $\text{Cu}_3\text{N}$  is due to the atmospheric  $\text{CO}_2$ . Also observed in both ODA and capped particles is the C–O stretching frequency. This suggests the presence of impurities in ODA possibly oxidation and this explains the presence of C–O in the XPS. A sharp peak was obtained at  $624.6\text{ cm}^{-1}$  which is very close to the  $639$ ,<sup>28</sup>  $\sim 650$  (ref. 6) and  $653\text{ cm}^{-1}$  (ref. 5) that were obtained in previous reports ascribed to Cu–N vibrations in copper(i) nitride.<sup>29</sup>

Wang and Li<sup>11</sup> suggested that the ODA does not participate in the reaction but rather acts as a catalyst that facilitates the transfer of electrons from  $\text{O}^{2-}$  to  $\text{Cu}^{2+}$  and  $\text{N}^{5+}$  of the nitrate. However, we are of the notion that ODA is most likely a participant in the reaction. In the FTIR, the symmetric and antisymmetric N–H vibration modes found at  $3259.5\text{ cm}^{-1}$  and  $3333\text{ cm}^{-1}$  respectively on the ODA spectrum were not detected on the  $\text{Cu}_3\text{N}$  spectrum. Instead, a new peak was spotted at  $2120\text{ cm}^{-1}$  and can be assigned to  $\text{C}\equiv\text{N}$  stretching vibration mode. In another study, this peak was detected at about  $2092\text{ cm}^{-1}$  and we agree with the authors who suggested the

possibility of the existence of  $\text{C}\equiv\text{N}$  due to the high temperature breakdown of ODA.<sup>10</sup>

To further probe this theory, the as-synthesized  $\text{Cu}_3\text{N}$  nanocubes and raw ODA were analyzed using proton nuclear magnetic resonance ( $^1\text{H}$  NMR). Analysis of the  $^1\text{H}$  NMR clearly revealed the deprotonation of the ODA ( $\text{CH}_3(\text{CH}_2)_{16}\text{CH}_2\text{-NH}_2$ ), resulting in the formation of stearonitrile ( $\text{CH}_3(\text{CH}_2)_{16}\text{C}\equiv\text{N}$ ). From the  $^1\text{H}$  NMR spectra in Fig. 7, the resonance for the  $\text{H}_3\text{C}$ -protons is centralized around  $\delta$  0.88 ppm in both the spectra of raw ODA and the  $\text{Cu}_3\text{N}$  NPs. At  $\delta$  1.25 and  $\delta$  1.26 ppm, a singlet is observed in both spectra and it accounts for protons that are on the  $\text{CH}_2$  chains respectively. Henceforth, notable differences were observed in the two spectra. In the raw ODA, a slightly broad triplet was observed centralized at  $\delta$  1.46 ppm but on the other hand, the spectrum that was obtained from the NPs showed a very broad peak with a peak maximum at  $\delta$  1.57 ppm. Thereafter, no further proton peaks were detected on the spectrum of the  $\text{Cu}_3\text{N}$  NPs but a triplet was obtained at  $\delta$  2.68 ppm on raw ODA and this accounted for the missing 2 H in the  $-\text{CH}_2$  that is directly bonded to the N on the amine end. These  $\text{CH}_2$  protons are clearly non-existent in the spectrum of the  $\text{Cu}_3\text{N}$  NPs. This is most probably because the H on the  $\text{H}_2\text{N-CH}_2-$  are all involved in the reaction that leads to the formation

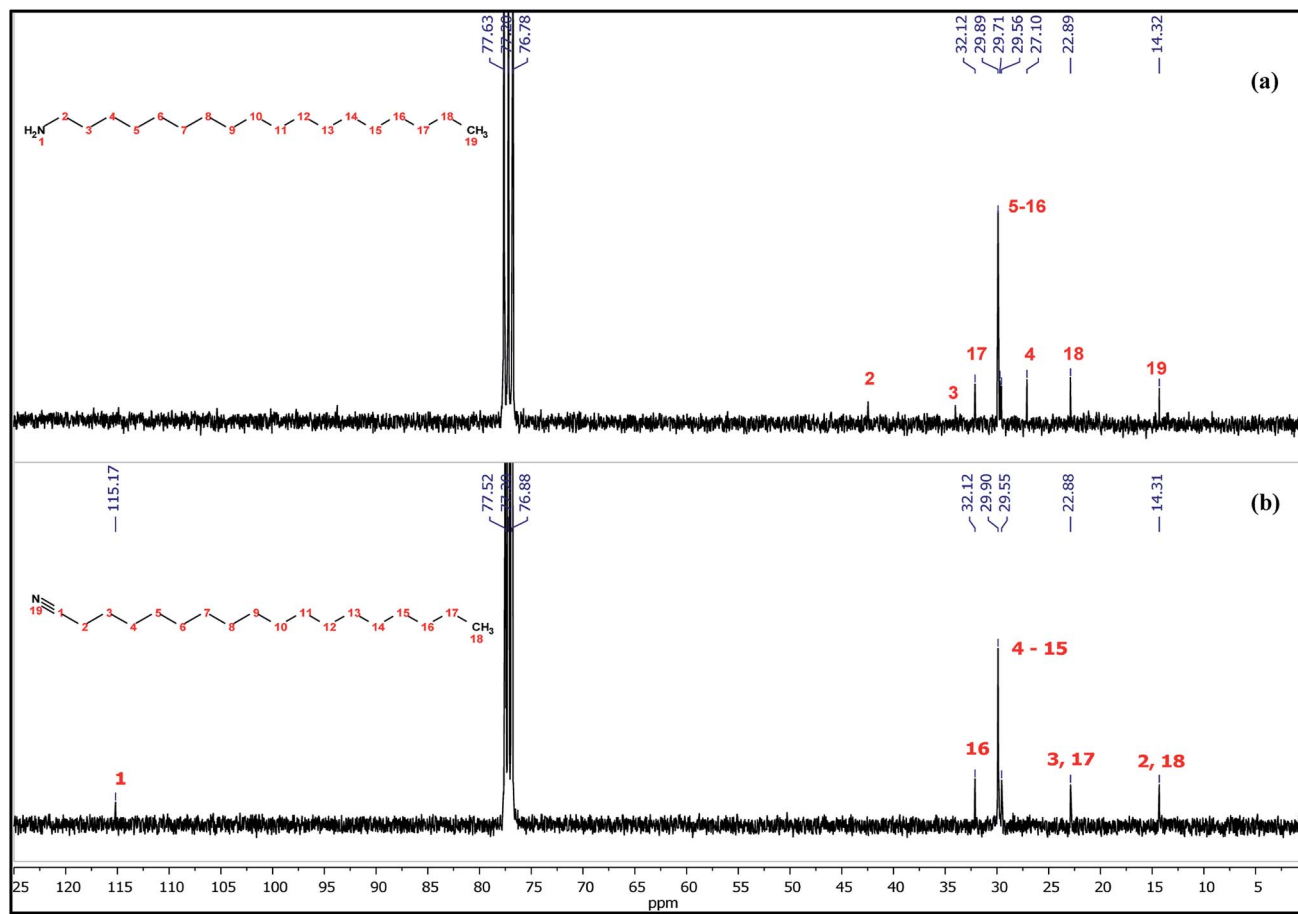
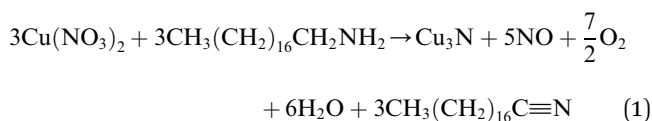


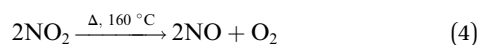
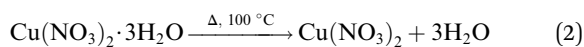
Fig. 9  $^{13}\text{C}$  NMR spectra of (a) ODA and (b)  $\text{Cu}_3\text{N}$  nanocubes in  $\text{CDCl}_3$  (15 min sample).

of  $\text{Cu}_3\text{N}$  NPs and stearonitrile remains as a by-product as depicted in the proposed chemical equation below:

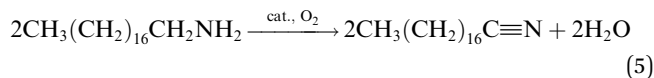


The formation of the stearonitrile is in agreement with the  $\text{C}\equiv\text{N}$  vibration modes that were detected at  $2120\text{ cm}^{-1}$  on the FTIR spectrum in Fig. 6. At temperatures above  $21.2\text{ }^\circ\text{C}$ ,  $\text{NO}_2$  is a reddish-brown gas with a pungent odor and it decomposes at about  $160\text{ }^\circ\text{C}$  (ref. 30) to give  $\text{NO}$  and  $\text{O}_2$  which are both colorless gases. To try and understand the full mechanism of the formation of the  $\text{Cu}_3\text{N}$  and the role of the expelled gases and ODA, the following processes are thought to be occurring during the reaction and these account for the overall eqn (1).

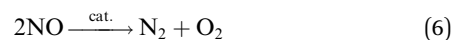
Decomposition of copper nitrate



Oxidation of octadecylamine



Decomposition of nitrous oxide



Formation of copper nitride



The breaking down of copper nitrate is common knowledge and results in the formation of  $\text{CuO}$  and  $\text{NO}$ . As shown on the  $^1\text{H}$  NMR in Fig. 7, the ODA is converted to stearonitrile. To check if indeed this occurs due to high temperature thermolysis as previously suggested,<sup>10</sup> ODA was heated from room temperature (RT) up to  $260\text{ }^\circ\text{C}$  under nitrogen and then analyzed with  $^1\text{H}$  NMR. The results are shown in Fig. 8.

The  $^1\text{H}$  NMR spectra in Fig. 8 show that at temperatures up to the synthetic temperature ( $260\text{ }^\circ\text{C}$ ), no oxidation of ODA occurs, however, at higher temperatures ( $310\text{ }^\circ\text{C}$ ) and longer reaction times this occurs. This suggests that in the current



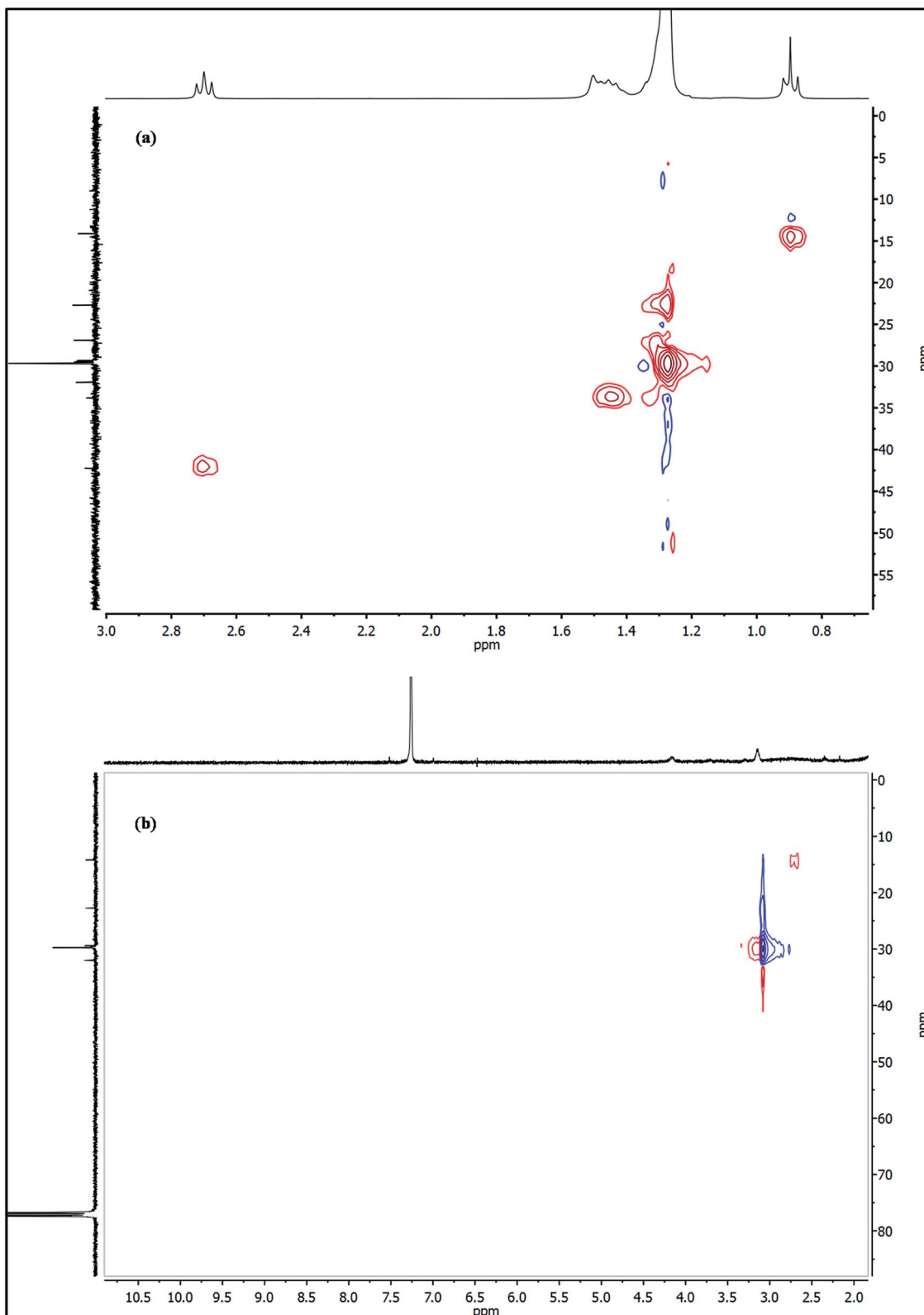


Fig. 10  $^1\text{H}$   $^{13}\text{C}$  HSQC NMR spectra of (a) ODA and (b)  $\text{Cu}_3\text{N}$  nanocubes (15 min) in  $\text{CDCl}_3$ .

study, the conversion of ODA to stearonitrile is not thermally driven; however, the oxidation is driven by the presence of a catalyst and oxygen in the reaction system. This is in

accordance with other studies where oxidation of a primary amine to nitrile has occurred using a catalyst in a presence of oxygen.<sup>31</sup> Herein, we therefore suggest that  $\text{CuO}$  catalyzes the

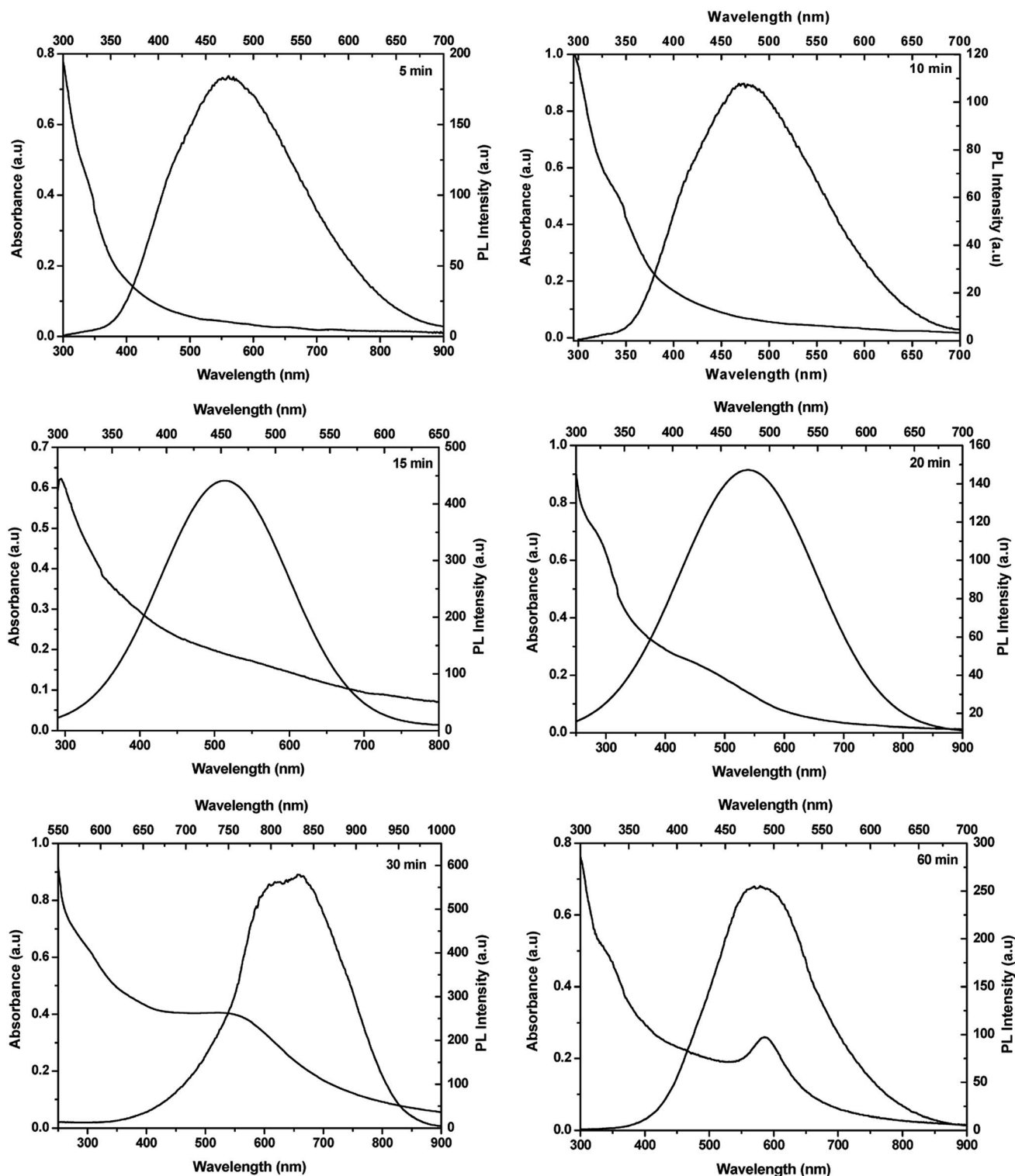


Fig. 11 UV-vis and PL spectra of  $\text{Cu}_3\text{N}$  NPs obtained at 5, 10, 15, 20, 30 and 60 min.

oxidation of ODA. At the same time, it catalyzes the decomposition of  $\text{NO}$  to  $\text{N}_2$  and  $\text{O}_2$ .<sup>32</sup> In the process of catalyzing these reactions, the  $\text{CuO}$  is then reduced to  $\text{Cu}$ . Finally  $\text{Cu}$  and  $\text{N}_2$  react to form  $\text{Cu}_3\text{N}$ . The reaction of  $\text{Cu}$  with  $\text{N}_2$  has been readily shown in the RF magnetron sputtering of  $\text{Cu}_3\text{N}$ ,<sup>33,34</sup> however

ultra-pure nitrogen gas is used. Herein, we therefore suggest that the  $\text{N}_2$  gas feed is merely to maintain an inert atmosphere and is not reactive. As such the  $\text{N}_2$  generated from the decomposition of  $\text{NO}$  is the reactive gas and a limiting reagent in the formation of  $\text{Cu}_3\text{N}$ . The process is shown from eqn (2)–(7).

Table 1 Summary of the optical properties of Cu<sub>3</sub>N NPs

Time (min)	Exciton A (nm)	Exciton A (eV)	Exciton B (nm)	Exciton B (eV)	$\lambda_{\max}$ (nm)	$\lambda_{\max}$ (eV)
5	476	2.61	—	—	476	2.61
10	456	2.72	—	—	476	2.61
15	436	2.84	—	—	455	2.73
20	378	3.28	608	2.04	478	2.59
30	340	3.65	760	1.63	832	1.49
60	400	3.10	695	1.78	487	2.55

The <sup>13</sup>C NMR spectra of raw ODA and ODA-capped Cu<sub>3</sub>N NPs are shown in Fig. 9. In both spectra, the <sup>13</sup>C signals of the methyl and methylene groups are detected around  $\delta$  14.32 and 22.89–32.12 ppm respectively. Of great interest is the huge downfield shift of the carbon peak at  $\delta$  42.46 in raw ODA to  $\delta$  115.17 ppm in the NPs which can be used as a diagnostic signal. The obtained 115.17 ppm in this study is lower than the 119.77 ppm that was obtained by Gunstone<sup>35</sup> when he was working with oleyl compounds but fall within the shift ranges of nitriles. This huge downfield shift is due to the deprotonation of the carbon that is bonded to nitrogen, H<sub>2</sub>C–NH<sub>2</sub> to form the nitrile (RCN). The appearance of the carbon peak at  $\delta$  115.17 ppm suggests the formation of a quaternary nitrile-bearing center hence, confirms the presence of octadecylnitrile in the Cu<sub>3</sub>N NPs. Due to the strong influence of the nitrile group, the nearby carbon atoms, C3 and C4 are greatly affected owing to  $\pi$ -electron deshielding and the polar inductive effect<sup>36</sup> of the nitrile group. As suggested in the equation above, the synthesis of Cu<sub>3</sub>N nanoparticles involves the process of deprotonation of octadecylamine to form octadecylnitrile. The nitrile group then forms sigma bonds with the Cu<sup>+</sup> ions resulting in end-on coordination hence accounting for the obtained down field shift at 115.17 ppm. If the coordination was side-on through the  $\pi$  system of the triple bond, a farther downfield resonance in the 180–240 ppm range would have been detected.<sup>37</sup>

The protons are matched to the carbon peaks as shown on the <sup>1</sup>H <sup>13</sup>C HSQC NMR spectra in Fig. 10a and b for both the ODA and Cu<sub>3</sub>N nanocubes respectively and all the protons and carbons are accounted for. This confirms that copper is in the oxidation state of 1+ since there are no unpaired electrons in the analyzed Cu<sub>3</sub>N NPs. If copper existed as Cu<sup>0</sup> or Cu<sup>2+</sup> in the analyzed Cu<sub>3</sub>N 'perfect' nanocubes that were obtained after 15 min, then the spectrum would not have been clearly resolved due to the unpaired electrons that exist in the 4s and 3d orbitals respectively.

The optical properties of the resultant Cu<sub>3</sub>N NPs were studied using UV-vis absorption and photoluminescence spectroscopy and the results are depicted in Fig. 11. In literature, there has been controversy with regards to the optical properties of Cu<sub>3</sub>N. From the varying band gap values obtained both theoretically and experimentally, they are said to vary between 0.23 eV and 2.06 eV, to the nature of the band gap transition whether it is direct or indirect.<sup>38,39</sup> Presented in Table 1 is the

summary of the optical properties. A single sharp excitonic peak is observed for 5 and 10 min samples whilst a tailing spectrum, also with a single excitonic peak is observed for the 15 min sample. Two peaks are observed for particles synthesized from 20 min to 60 min. From band structure calculations, three transitions have been reported, one indirect and two direct band gaps at the  $\Gamma$  and R points.<sup>39</sup> The exciton A is blue-shifted from the reported values and the transition is in the visible region of the electromagnetic spectrum whilst exciton B is consistent with the reported values with the band gap energies of 1.6–2.04 eV. The observed trends could be because of quantum confinement effects in the nanocrystals as most reported results are for bulk Cu<sub>3</sub>N.<sup>38,39</sup> Also possible, is the presence of the localized surface plasmon resonance (LSPR) due to the presence of copper nanoparticles. The LSPR for Cu nanoparticles is usually found around 570 nm and can be blue or red shifted due to the size and shape of the nanoparticles, the photoluminescence is usually weak hence the observed photoluminescence peaks are only associated with the semi-conducting Cu<sub>3</sub>N NPs.<sup>40</sup>

The photoluminescence spectra are red-shifted with respect to the excitonic peak A for samples synthesized for 10–20 min as well as 60 min however for the 30 min sample the emission maximum correlates with the exciton B transition. The photoluminescence spectra confirm that the resultant nanoparticles are direct band gap semiconductors. Evident from the results is the complexity of the optical properties and the need to further probe these. Based on the obtained results, it is quite evident that Cu<sub>3</sub>N is an interesting and rather complex semiconductor. Nevertheless, herein using TEM, a mechanism for the evolution of Cu<sub>3</sub>N morphologies can be postulated and it is depicted in Fig. 12. The reaction was started by dissolution of Cu(NO<sub>3</sub>)<sub>2</sub>·3H<sub>2</sub>O in OD and mixed with ODA and then the temperature was raised from room temperature to 110 °C resulting in a deep blue mixture. After an hour, the temperature was slowly increased and at about 165 °C, a very pale yellow clear solution was obtained. This could be a result of the formation of a complex between the Cu(I) ions and octadecylamine as has been observed in a previous study.<sup>10</sup> The blue coloration that was caused by the unpaired electron in the Cu<sup>2+</sup> suddenly disappeared due to the reduction of Cu<sup>2+</sup> to Cu<sup>+</sup> in the presence of ODA. Due to complete d orbital, Cu<sup>+</sup> does not give off color hence the yellow color is brought about by the complexation that occurs between the Cu(I) ions and the amine. The solution then slowly turned to a clear brown around 200 °C and then to an opaque brown by the time the temperature reached 260 °C. It has been shown that in direct heating methods, high quality crystals are generally obtained at high temperatures that are above 200 °C hence 260 °C was chosen as the reaction temperature in this study. The introduction of the brown color indicates the initial stages of the formation of Cu<sub>3</sub>N nuclei. An attempt to analyze the samples that were obtained after 30 s at 260 °C proved futile as the aliquots turned greenish blue upon adding organic solvents like ethanol or chloroform in an attempt to clean the NPs. This color change indicated the oxidation of the Cu<sup>+</sup> to Cu<sup>2+</sup>. There was no marked difference between the NPs obtained after 1 min and those obtained at

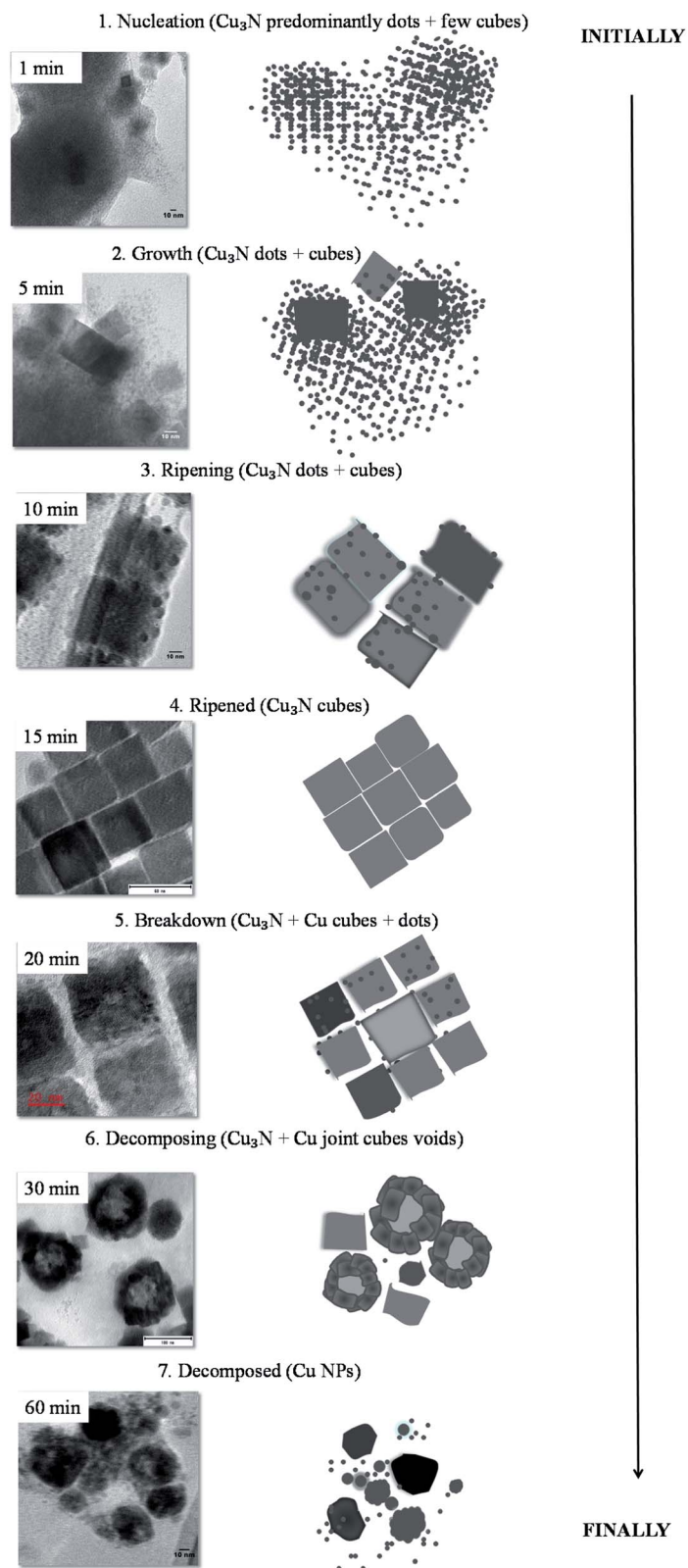


Fig. 12 Steps followed in the colloidal thermolysis of  $\text{Cu}(\text{NO}_3)_2$  in ODA to form  $\text{Cu}_3\text{N}$  NPs and eventually Cu.

5 min except that there were more defined nanocubes at 5 min as compared to 1 min as seen in Fig. 12. As such, below 1 min, the nuclei that had formed were not yet stable and reacted

rapidly with air and the added solvent. ODA has been reported as having a tendency to bind to the 100 plane of  $\text{Cu}_3\text{N}$  NPs hence it slows down the growth process and facilitates the formation

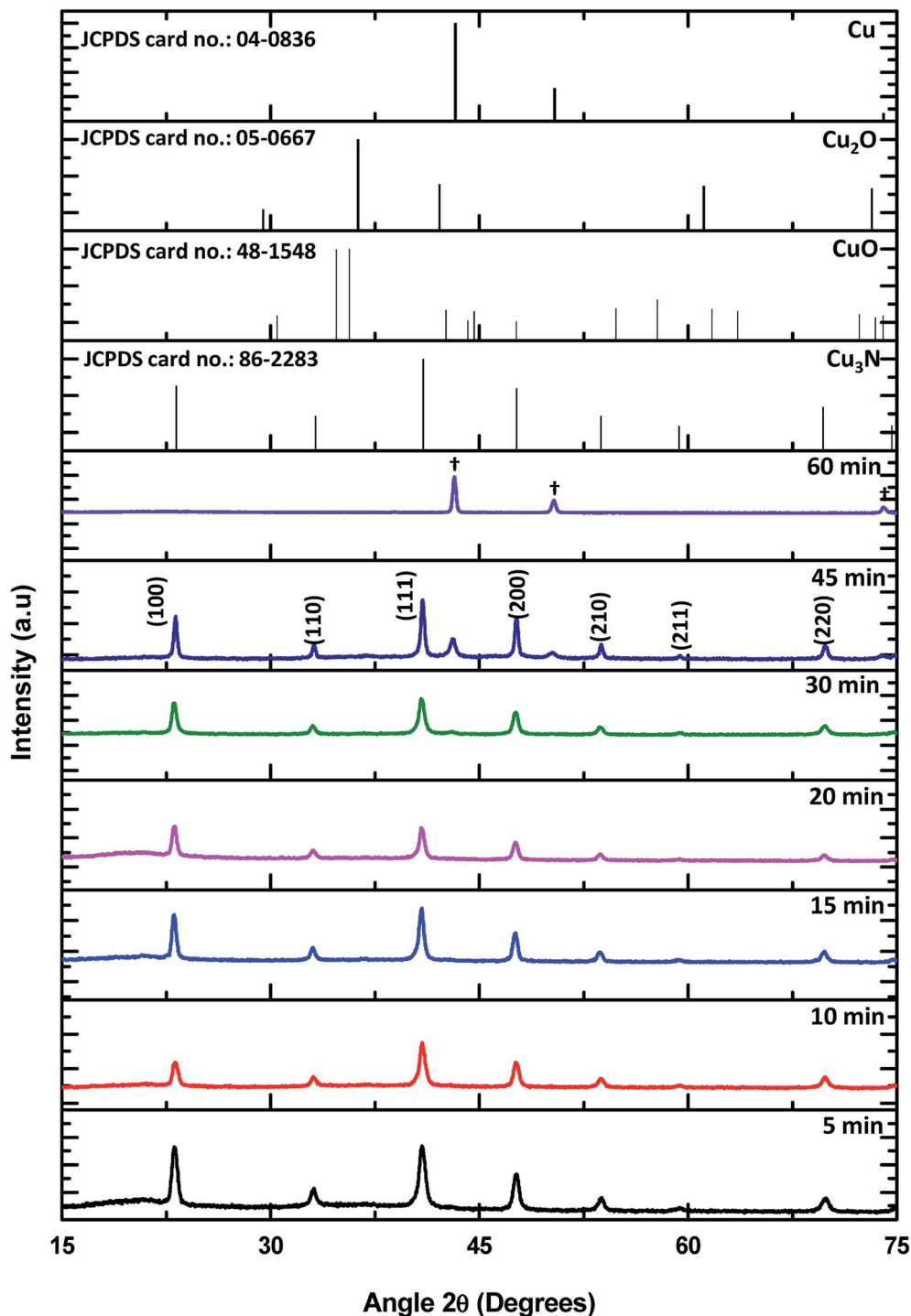


Fig. 13 Powder XRD of Cu<sub>3</sub>N NPs obtained after (a) 5, 10, 15, 20, 30, 45 and 60 min at 260 °C in HDA. The symbol (†) shows peaks for Cu decomposition product of the capping agent.

of cubes.<sup>10</sup> High population of 'dots' were detected in the 5 min sample while few cubes had already been formed although not fully developed. The less stable small nanocrystals undergo Oswald ripening<sup>41</sup> as they slowly dissolve and recrystallize on the larger particles giving rise to nanocubes. This was observed at 10 min where self-assembly of cubes was noted and fewer but bigger dots were seen on and in-between the cubes. Subsequent

ripening or shaping led to the formation of the 'perfect' nanocubes with smooth edges and no apparent blemishes at 15 min. Continued heating resulted in further reduction which led to the detected small peak of Cu in the XRD of the 20 min sample. The reduction of the copper ions on the surface of the cubes led to the influx of Cu<sup>+</sup> ions from the core to the surface of the nanocubes.<sup>42</sup> As such, the smooth surface that had been

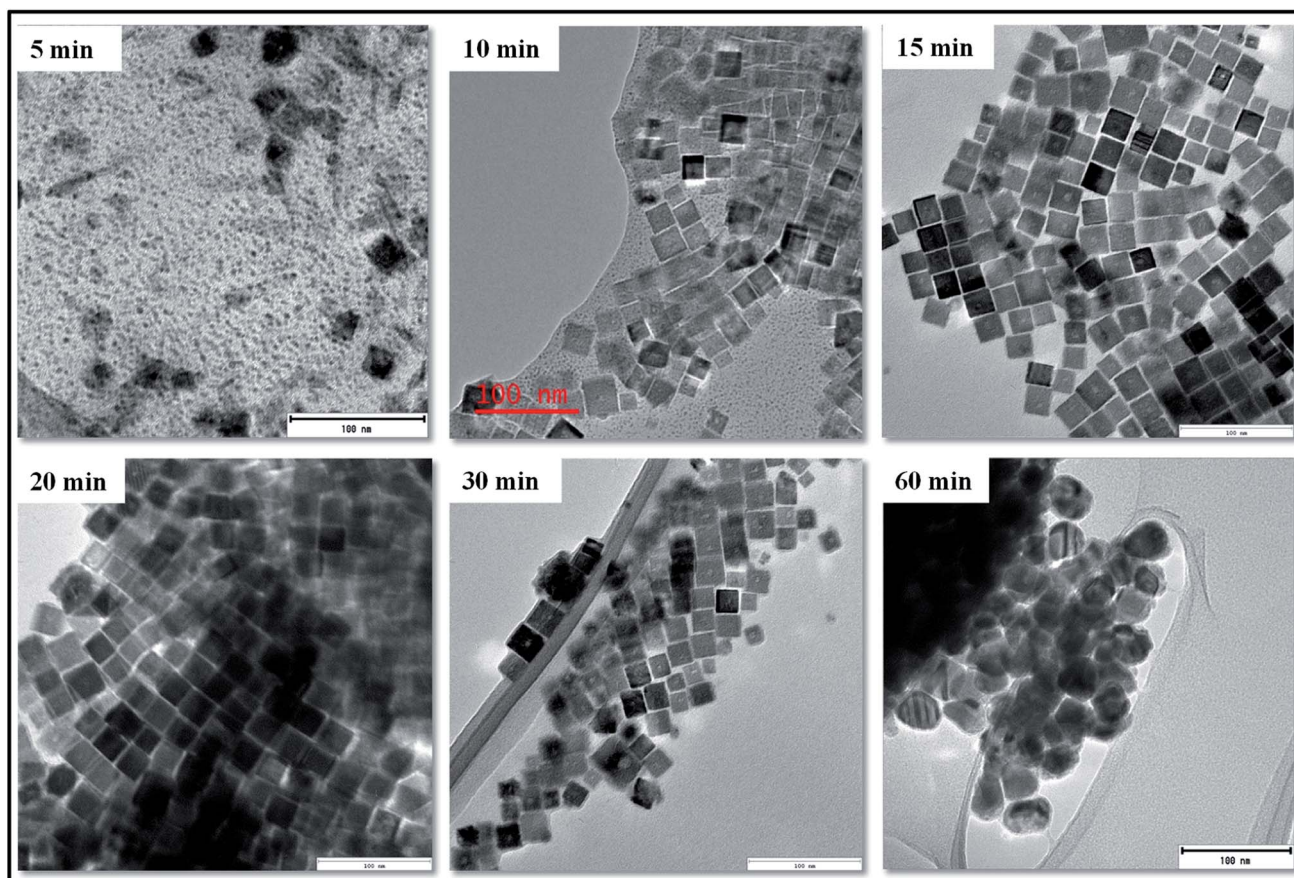


Fig. 14 TEM images of  $\text{Cu}_3\text{N}$  NPs obtained after 5, 10, 15, 20 and 30 min and Cu at 60 min in HDA at 260 °C.

observed on the 'perfect' nanocubes could no longer hold on the NPs that were obtained at 20 min. The cationic movement of  $\text{Cu}^+$  from the core of the cubes to the edges continued and voids can be seen in the interior of the distorted cubes, consequently resulting in the reemission of nitrogen. As the cubes broke down, they joined together to form larger cubes with void interiors. That is why at this stage, pronounced Cu peaks could be detected at 30 min as  $\text{Cu}_3\text{N}$  decomposed and the  $\text{Cu}^+$  was reduced to  $\text{Cu}^0$  whilst the  $\text{N}^{3-}$  was oxidized to nitrogen gas. Finally with time, 'all'  $\text{Cu}_3\text{N}$  had been reduced to Cu hence no copper nitride peaks could be detected after 60 min.

To determine if this is a unique feature to octadecylamine, the coordinating ligand was changed from ODA to hexadecylamine (HDA). The same synthetic procedure was followed and the resultant X-ray diffractograms are shown in Fig. 13.

The XRD diffractograms showed a similar pattern with the one obtained in ODA, the main difference being the initial detection of Cu occurring after 30 min whilst in ODA it was detected at 20 min. This difference was seen in the TEM images of the NPs that were obtained in HDA. 'Perfect' nanocubes could be seen at 15 min but not much variation was detected in the 20 min sample. Mixed morphology of nanocubes and tiny dot-like NPs were clearly seen in the 5 and 10 min samples and breaking down of the nanocubes was only detected after 30 min. Just like in ODA, compact Cu NPs were obtained after 60 min

and no nanocubes could be seen (Fig. 14). The  $^1\text{H}$  NMR and  $^{13}\text{C}$  NMR of HDA shown in Fig. 2S and 3S<sup>†</sup> respectively were similar to the ODA NMR and therefore the mechanism was consistent with ODA.

## 4. Conclusion

The thermal decomposition of  $\text{Cu}(\text{NO}_3)_2$  at 260 °C in ODA lead to the formation of dot-like nuclei which resulted in the formation of  $\text{Cu}_3\text{N}$  nanocubes. A cloud of  $\text{Cu}_3\text{N}$  nuclei with developing nanocubes was obtained after 5 min. Aligned nanocubes were seen at 10 min with the presence of bigger but fewer 'dots'. With time, well-defined  $\text{Cu}_3\text{N}$  nanocubes were obtained after 15 min and this was observed in both ODA and HDA. Further heating resulted in the breaking down of the nanocubes and XRD indicated the presence of both  $\text{Cu}_3\text{N}$  and Cu at 30 min. By 60 min, the  $\text{Cu}_3\text{N}$  had completely decomposed to Cu. Furthermore, results from the FTIR and NMR spectroscopy suggested the formation of a nitrile (RCN) as a product in the synthesis of  $\text{Cu}_3\text{N}$  in ODA and that the particles are possibly capped by the nitrile. The proposed mechanism suggests that the  $\text{Cu}_3\text{N}$  NPs dorms from the reaction of Cu with  $\text{N}_2$ , however this requires further experimental probing. The optical studies revealed that the as-synthesized nanoparticles were semi-conducting with two transitions observed in the UV-vis

absorption spectra. The synthesized  $\text{Cu}_3\text{N}$  NPs can potentially be applied as microscopic metallic links due to its metallization at relatively low temperatures.

## Conflicts of interest

There are no conflicts to declare.

## Acknowledgements

The authors would like to acknowledge the National Research Foundation (South Africa) and the University of the Witwatersrand. The authors' gratitude is duly directed to the Microscopy Unit (MMU) at Wits for the TEM and XRD analysis.

## References

- 1 Z. Cao, *Thin film growth: physics, materials science and applications*, Woodhead Publishing Limited, 2011.
- 2 T. Nakamura, N. Hiyoshi, H. Hayashi and T. Ebina, Preparation of plate-like copper nitride nanoparticles from a fatty acid copper (II) salt and detailed observations by high resolution transmission electron microscopy and high-angle annular dark-field scanning transmission electron microscopy, *Mater. Lett.*, 2015, **139**, 271–274.
- 3 T. Nakamura, H. Hayashi, T.-A. Hanaoka and T. Ebina, Preparation of copper nitride ( $\text{Cu}_3\text{N}$ ) nanoparticles in long-chain alcohols at 130 – 200 °C and nitridation mechanism, *Inorg. Chem.*, 2013, **53**, 710–715.
- 4 M. D. Reichert, M. A. White, M. J. Thompson, G. J. Miller and J. Vela, Preparation and instability of nanocrystalline cuprous nitride, *Inorg. Chem.*, 2015, **54**, 6356–6362.
- 5 R. Szczesny, E. Szyk, M. A. Wisniewski, T. K. Hoang and D. H. Gregory, Facile preparation of copper nitride powders and nanostructured films, *J. Mater. Chem. C*, 2016, **4**, 5031–5037.
- 6 J. Choi and E. Gillan, Solvothermal synthesis of nanocrystalline copper nitride from an energetically unstable copper azide precursor, *Inorg. Chem.*, 2005, **44**, 7385.
- 7 S. Mondal and C. R. Raj, Copper nitride nanostructure for the electrocatalytic reduction of oxygen: kinetics and reaction pathway, *J. Mater. Chem. C*, 2018, **122**, 18468–18475.
- 8 T. Nakamura, H. Hayashi and T. Ebina, Preparation of copper nitride nanoparticles using urea as a nitrogen source in a long-chain alcohol, *J. Nanoparticle Res.*, 2014, **16**, 2699.
- 9 Z.-Q. Liang, T.-T. Zhuang, A. Seifitokaldani, J. Li, C.-W. Huang, C.-S. Tan, Y. Li, P. De Luna, C. T. Dinh and Y. Hu, Copper-on-nitride enhances the stable electrosynthesis of multi-carbon products from  $\text{CO}_2$ , *Nat. Commun.*, 2018, **9**, 1–8.
- 10 H. Wu and W. Chen, Copper nitride nanocubes: size-controlled synthesis and application as cathode catalyst in alkaline fuel cells, *J. Am. Chem. Soc.*, 2011, **133**, 15236–15239.
- 11 D. Wang and Y. Li, Controllable synthesis of Cu-based nanocrystals in ODA solvent, *Chem. Commun.*, 2011, **47**, 3604–3606.
- 12 R. K. Sithole, L. F. Machogo, M. A. Airo, S. S. Gqoba, M. J. Moloto, P. Shumbula, J. Van Wyk and N. Moloto, Synthesis and characterization of  $\text{Cu}_3\text{N}$  nanoparticles using pyrrole-2-carbaldpropyliminato Cu (II) complex and  $\text{Cu}(\text{NO}_3)_2$  as single-source precursors: the search for an ideal precursor, *New J. Chem.*, 2018, **42**, 3042–3049.
- 13 P. Xi, Z. Xu, D. Gao, F. Chen, D. Xue, C.-L. Tao and Z.-N. Chen, Solvothermal synthesis of magnetic copper nitride nanocubes with highly electrocatalytic reduction properties, *RSC Adv.*, 2014, **4**, 14206–14209.
- 14 D. S. Wang, T. Xie, Q. Peng, S. Y. Zhang, J. Chen and Y. D. Li, Direct thermal decomposition of metal nitrates in octadecylamine to metal oxide nanocrystals, *Chem. - Eur. J.*, 2008, **14**, 2507–2513.
- 15 T. Maruyama and T. Morishita, Copper nitride and tin nitride thin films for write-once optical recording media, *Appl. Phys. Lett.*, 1996, **69**, 890–891.
- 16 R. Cremer, M. Witthaut, D. Neuschütz, C. Trappe, M. Laurenzis, O. Winkler and H. Kurz, Deposition and Characterization of Metastable  $\text{Cu}_3\text{N}$  Layers for Applications in Optical Data Storage, *Microchim. Acta*, 2000, **133**, 299–302.
- 17 A. Majumdar, S. Drache, H. Wulff, A. K. Mukhopadhyay, S. Bhattacharyya, C. A. Helm and R. Hippler, Strain effects by surface oxidation of  $\text{Cu}_3\text{N}$  thin films deposited by DC magnetron sputtering, *Coatings*, 2017, **7**, 64.
- 18 X. Fan, Z. Wu, H. Li, B. Geng, C. Li and P. Yan, Morphology and thermal stability of Ti-doped copper nitride films, *J. Phys. D: Appl. Phys.*, 2007, **40**, 3430.
- 19 A. Fallberg, M. Ottosson and J. O. Carlsson, CVD of copper(I) nitride, *Chem. Vap. Deposition*, 2009, **15**, 300–305.
- 20 C. Navio, M. Capitan, J. Alvarez, F. Yndurain and R. Miranda, Intrinsic surface band bending in  $\text{Cu}_3\text{N}$  (100) ultrathin films, *Phys. Rev. B: Condens. Matter Mater. Phys.*, 2007, **76**, 085105.
- 21 L.-C. Wang, B.-H. Liu, C.-Y. Su, W.-s. Liu, C.-C. Kei, K.-W. Wang and T.-P. Perng, Electronic band structure and electrocatalytic performance of  $\text{Cu}_3\text{N}$  nanocrystals, *ACS Appl. Nano Mater.*, 2018, **1**(7), 3673–3681.
- 22 M. Trivedi, G. Singh, A. Kumar and N. P. Rath, A cyano and end-to-end azido bridged 3D copper (II)–copper (I) mixed-valence coordination polymer and its transformation to copper nitride nanoparticles, *RSC Adv.*, 2014, **4**, 34110–34116.
- 23 A. Miura, T. Takei and N. Kumada, Synthesis of  $\text{Cu}_3\text{N}$  from  $\text{CuO}$  and  $\text{NaNH}_2$ , *J. Asian Ceram. Soc.*, 2014, **2**, 326–328.
- 24 A. K. Mukhopadhyay, A. Roy, S. C. Das, H. Wulff, R. Hippler and A. Majumdar, Self-buckled effect of cubic  $\text{Cu}_3\text{N}$  film: Surface stoichiometry, in *AIP Conference Proceedings*, AIP Publishing, 2018, p. 100078.
- 25 O. Akhavan, R. Azimirad, S. Safa and E. Hasani,  $\text{CuO}/\text{Cu}(\text{OH})_2$  hierarchical nanostructures as bactericidal photocatalysts, *J. Mater. Chem.*, 2011, **21**, 9634–9640.
- 26 M. Younas, J. Shen, M. He, R. Lortz, F. Azad, M. Akhtar, A. Maqsood and F. C. Ling, Role of multivalent Cu, oxygen

- vacancies and CuO nanophase in the ferromagnetic properties of ZnO: Cu thin films, *RSC Adv.*, 2015, **5**, 55648–55657.
- 27 J. Wang, Q. Deng, M. Li, K. Jiang, J. Zhang, Z. Hu and J. Chu, Copper ferrites@ reduced graphene oxide anode materials for advanced lithium storage applications, *Sci. Rep.*, 2017, **7**, 8903.
- 28 R. Deshmukh, G. Zeng, E. Tervoort, M. Staniuk, D. Wood and M. Niederberger, Ultrasmall Cu<sub>3</sub>N nanoparticles: surfactant-free solution-phase synthesis, nitridation mechanism, and application for lithium storage, *Chem. Mater.*, 2015, **27**, 8282–8288.
- 29 J. Choi and E. G. Gillan, Solvothermal metal azide decomposition routes to nanocrystalline metastable nickel, iron, and manganese nitrides, *Inorg. Chem.*, 2009, **48**, 4470–4477.
- 30 R. P. Pohanish, *Sittig's Handbook of Toxic and Hazardous Chemicals and Carcinogens*, William Andrew, 2008.
- 31 Q. Sun, Z. Wang, D. Wang, Z. Hong, M. Zhou and X. Li, A review on the catalytic decomposition of NO to N<sub>2</sub> and O<sub>2</sub>: catalysts and processes, *Catal. Sci. Technol.*, 2018, **8**, 4563–4575.
- 32 O. D. Pavel, P. Goodrich, L. Cristian, S. M. Coman, V. I. Pârvulescum and C. Hardacre, Direct oxidation of amines to nitriles in the presence of ruthenium-terpyridyl complex immobilized on ILs/SILP, *Catal. Sci.*, 2015, **5**, 2696–2704.
- 33 J. Wang, J. T. Chen, X. M. Yuan, Z. G. Wu, B. B. Miao and P. X. Yan, Copper nitride (Cu<sub>3</sub>N) thin films deposited by RF magnetron sputtering, *J. Cryst. Growth*, 2006, **286**, 407–412.
- 34 C. M. Caskey, R. M. Richards, D. S. Ginley and A. Zakutayev, Thin film synthesis and properties of copper nitride, a metastable semiconductor, *Mater. Horiz.*, 2014, **1**, 424–430.
- 35 F. Gunstone, High-resolution <sup>13</sup>C NMR spectra of long-chain acids, methyl esters, glycerol esters, wax esters, nitriles, amides, alcohols and acetates, *Chem. Phys. Lipids*, 1993, **66**, 189–193.
- 36 R. J. Abraham and M. Reid, Proton chemical shifts in NMR. Part 15-proton chemical shifts in nitriles and the electric field and π-electron effects of the cyano group, *Magn. Reson. Chem.*, 2000, **38**, 570–579.
- 37 A. B. Jackson, Nitrile reduction and carbon monoxide replacement in tungsten(II) bis(acetylacetonate) complexes, PhD dissertation, The University of North Carolina at Chapel Hill, 2008.
- 38 U. Hahn and W. Weber, Electronic structure and chemical-bonding mechanism of Cu<sub>3</sub>N, CuI<sub>3</sub>NPd, and related Cu (I) compounds, *Phys. Rev. B: Condens. Matter Mater. Phys.*, 1996, **53**, 12684.
- 39 M. Mikula, D. Búć and E. Pincik, Electrical and optical properties of copper nitride thin films prepared by reactive DC magnetron sputtering, *Acta Phys. Slovaca*, 2000, **51**, 35–43.
- 40 O. A. Yeshchenko, I. S. Bondarchuk and M. Yu. Losytskyy, Surface plasmon enhanced photoluminescence from copper nanoparticles: Influence of temperature, *J. Appl. Phys.*, 2014, **116**, 054309.
- 41 M. Mlambo, M. J. Moloto, N. Moloto and P. S. Mdluli, Influence of temperature and precursor concentration on the synthesis of HDA-capped Ag<sub>2</sub>Se nanoparticles, *Mater. Res. Bull.*, 2013, **48**(6), 2196–2200.
- 42 A. Bruckman and G. Simkovich, Concerning the mechanism of scale growth due to cation diffusion in Fe<sub>2</sub>O<sub>3</sub> and CuS, *Corros. Sci.*, 1972, **12**, 595–601.